

Multiscaling behavior of atomic-scale frictionM. Jannesar,¹ T. Jamali,² A. Sadeghi,^{3,4} S. M. S. Movahed,³ G. Fesler,⁵ E. Meyer,⁵ B. Khoshnevisan,¹ and G. R. Jafari³¹*Department of Physics, Kashan University, Kashan 8731751167, Iran*²*School of Physics, Institute for Research in Fundamental Sciences (IPM), P.O. Box 19395-5531, Tehran, Iran*³*Department of Physics, Shahid Beheshti University, G.C., Evin, Tehran 19839, Iran*⁴*School of Nano Science, Institute for Research in Fundamental Sciences (IPM), Tehran 19395-5531, Iran*⁵*Departement Physik, Universität Basel, Klingelbergstr. 82, 4056 Basel, Switzerland*

(Received 5 August 2016; revised manuscript received 10 May 2017; published 19 June 2017)

The scaling behavior of friction between rough surfaces is a well-known phenomenon. It might be asked whether such a scaling feature also exists for friction at an atomic scale despite the absence of roughness on atomically flat surfaces. Indeed, other types of fluctuations, e.g., thermal and instrumental fluctuations, become appreciable at this length scale and can lead to scaling behavior of the measured atomic-scale friction. We investigate this using the lateral force exerted on the tip of an atomic force microscope (AFM) when the tip is dragged over the clean NaCl (001) surface in ultra-high vacuum at room temperature. Here the focus is on the fluctuations of the lateral force profile rather than its saw-tooth trend; we first eliminate the trend using the singular value decomposition technique and then explore the scaling behavior of the detrended data, which contains only fluctuations, using the multifractal detrended fluctuation analysis. The results demonstrate a scaling behavior for the friction data ranging from 0.2 to 2 nm with the Hurst exponent $H = 0.61 \pm 0.02$ at a 1σ confidence interval. Moreover, the dependence of the generalized Hurst exponent, $h(q)$, on the index variable q confirms the multifractal or multiscaling behavior of the nanofriction data. These results prove that fluctuation of nanofriction empirical data has a multifractal behavior which deviates from white noise.

DOI: [10.1103/PhysRevE.95.062802](https://doi.org/10.1103/PhysRevE.95.062802)**I. INTRODUCTION**

The recent trend of new technologies toward fabricating nanoscale devices demands a better understanding of physical phenomena at this scale. One of the phenomena, inherent in any physical system of contacting parts, is friction [1], which is present in a wide range of length scales [2,3]. Tribological studies at nano- and atomic scale are essential for completing the picture of this scaling quantity and explaining its complex behavior [4–6].

Since three decades ago, with the development of atomic force microscopy (AFM), experimental studies on friction at the atomic scale has become possible [1–3,6,7]. The friction force in a typical nanofriction experiment is determined from the lateral deflection of the AFM cantilever when the AFM tip is dragged across an atomically flat surface [8]. Numerous studies on the surface of various materials have shown a sawtooth-like pattern for nanofriction [9,10]. This behavior, which comes from the stick-slip motion of the tip, can be well described by the very basic Prandtl-Tomlinson model (a pointlike tip subject to a sinusoidal potential and dragged via a harmonic spring) [11,12]. The model has been extended to capture finite temperature effects [13–15]. The common approaches are using the master equation for the temporal evolution of the probability of thermally activating the tip [16] and the Langevin equation for the tip motion in which thermal effects are modeled by a Gaussian white-noise term [13]. These approaches justify the nanofriction thermal behavior to a great extent [17–19], although other fluctuation sources such as tip-apex instability, lattice deficiencies, and instrumental noises have been neglected.

Recently the effects of such neglected types of noises on the atomic-scale friction have been investigated. Labuda *et al.* [20–22] divided noises of a typical AFM experiment into

three categories: (1) detection noise which comes from AFM optical device, (2) force noise that is mainly caused by thermal fluctuations, and (3) displacement noise which is related to the design of AFM system. Their study was based on analyzing the noises of nanofriction data using the method of power spectral density and simulating the effect of each of these noises on nanofriction. Furthermore, Dong *et al.* [23,24] considered the effect of thermal and instrumental noises on the theoretical modeling of nanofriction using the master equation method.

The aim of this work is to look for any scaling behavior of the fluctuations present in the signal measured as friction by AFM experiments. As a next step, it will be interesting to investigate the individual contributions from the three above mentioned sources into the scaling behavior of the fluctuation either experimentally or by computer simulations. Here, however, we study the overall stochastic part of the experimental friction data that contains the effect of all noise sources together. To do so, we first remove the deterministic part of the data, i.e., the sawtooth-like trend, which comes from the periodic structure of the sublayer lattice, using the singular value decomposition (SVD) technique, and then we investigate the scaling behavior of the remaining noisy part using multifractal detrended fluctuation analysis (MF-DFA). We calculate the generalized scaling exponent that describes the multifractal properties of the nanofriction data. The results show that the share of all noises in the data is a multifractal signal with long-range correlation and thus cannot be replaced by a white noise on friction modeling.

The rest of this paper is organized as follows. Section II describes a brief review of the fluctuation analysis and detrending methods. Section III explains the details of the nanofriction experiment. A description of the data is also given here. Section IV presents the scaling behavior and

multifractality of the nanofriction data. In the final section we draw conclusions and summarize the work.

II. METHODS

A. Multifractal detrended fluctuation analysis

Real data sets coming from experiments are usually affected by nonstationarity and trends. Data reduction and cleaning procedures should be implemented in order to find reliable results by applying robust methods in the context of the data analysis approach. Extracting various scaling exponents on a statistical physics basis is known as a robust analysis method in order to determine the statistical properties and to identify the universality class of the underlying processes. To this end, a multiscaling algorithm in the presence of unknown trends and noises is one of the most reliable approach introduced and implemented in many previous studies. Multifractal detrended fluctuation analysis (MF-DFA) [25] is a widely used technique to study the multifractal scaling properties of nonstationary time series [26–30]. MF-DFA is the generalization of the detrended fluctuation analysis (DFA) [31]. For a typical series $\{x_i\}$ $i = 1, \dots, N$ with an insignificant fraction of zeros, the five steps are as follows:

(1) As a first step the so-called profile should be determined accordingly by integrating the original series $\{x\}$ as

$$X(j) = \sum_{i=1}^j x(i), \quad j = 1, \dots, N. \quad (1)$$

(2) Then we divide the series $\{X\}$ into $N_s = \text{int}(N/s)$ nonoverlapping segments of length s , which can take the value from 2 to $N/2$. In the case of remaining unused part of data from the end of series the procedure must be repeated from the opposite end in order to take into account the remaining data at the end of series.

(3) Compute the variance of fluctuations for each segment after subtracting the local trend in that segment as

$$F^2(s, n) = \frac{1}{s} \sum_{i=1}^s \{X[i + (n-1)s] - y_n(i)\}^2 \quad (2)$$

for segments $n = 1, \dots, N_s$ and

$$F^2(s, n) = \frac{1}{s} \sum_{i=1}^s \{X[i + N - (n - N_s)s] - y_n(i)\}^2 \quad (3)$$

for segments $n = N_s + 1, \dots, 2N_s$. Here $y_n(i)$ is a polynomial function describing the local trend in the n th segment. The order of polynomial function “ m ” fitted to the series $\{X\}$ determines which type of trend is eliminated in each segment. MF-DFA $_m$ denotes that the order of polynomial function used in MF-DFA is “ m .” Throughout this paper we take $m = 1$.

(4) Determine the q th-order fluctuation function by averaging over all segments

$$F_q(s) = \left\{ \frac{1}{2N_s} \sum_{n=1}^{2N_s} [F^2(s, n)]^{q/2} \right\}^{1/q}, \quad (4)$$

where the index parameter q can take any real value except zero. For the case $q = 0$ we have

$$F_0(s) = \exp \left[\frac{1}{4N_s} \sum_{n=1}^{2N_s} \ln F(s, n) \right]. \quad (5)$$

Note that ($q = 2$) gives the DFA, which is nothing but the second-order moment (i.e., variance). Calculating higher order moments helps to characterize the multifractality nature of series. Multifractal time series, contrary to monofractal series, contains both extremely small and large local fluctuations. Depending on the value and sign of the parameter q we can magnify the contribution of small and large fluctuations $F^2(s, n)$ in $F_q(s)$. In other words, this is a quantitative description of various values of fluctuations.

(5) Determine the scaling behavior of the fluctuation function $F_q(s)$ by analyzing its behavior for each value of q . For the series $\{x\}$ with self-similar behavior, $F_q(s)$ is an increasing function of s with the asymptotic power-law behavior

$$F_q(s) \sim s^{h(q)}. \quad (6)$$

If the scaling exponent $h(q)$ depends on q , the time series is multifractal, while for a monofractal time series, $h(q)$ is constant. Since for a stationary time series $h(q = 2)$ gives the standard Hurst exponent H , the scaling exponent $h(q)$ is called the generalized Hurst exponent. For a nonstationary time series like fractional Brownian motion $h(q) > 1$ and $h(q = 2)$ is no longer identical to the Hurst exponent H , but instead we have $H = h(q = 2) - 1$. The Hurst exponent H characterizes the correlation property of the time series [32–35]. For example, $H = 0.5$ shows that the time series is a white noise. $0 < H < 0.5$ and $0.5 < H < 1$ indicate antipersistence (negative correlation) and persistence (positive correlation) of the time series, respectively.

MF-DFA is related to the standard multifractal analysis through the partition function [25]

$$Z_q(s) \equiv \sum_{n=1}^{N_s} |X(ns) - X[(n-1)s]|^q \sim s^{\tau(q)}. \quad (7)$$

It can be proved that the scaling exponent $\tau(q)$ in Eq. (16) is related to the multifractal scaling exponent $h(q)$ as [25]

$$\tau(q) = qh(q) - 1. \quad (8)$$

This equation indicates that the exponent $\tau(q)$ for a monofractal series is linear. There is also a correspondence between the scaling exponent $\tau(q)$ and the singularity spectrum $f(\alpha)$ via the Legendre transform as [36]

$$\alpha = \frac{d\tau(q)}{dq} \quad \text{and} \quad f(\alpha) = \alpha q - \tau(q). \quad (9)$$

Another capability of MF-DFA as we expect is giving a quantitative measure for multifractality nature of underlying data sets. Accordingly, for a multifractal series, various parts of the feature are characterized by different values of α , resulting a set of Hölder exponents instead of a single α . Corresponding domain for Hölder spectrum, $\alpha \in [\alpha_{\min}, \alpha_{\max}]$, becomes

$$\alpha_{\min} = \lim_{q \rightarrow +\infty} \frac{\partial \tau(q)}{\partial q}, \quad (10)$$

$$\alpha_{\max} = \lim_{q \rightarrow -\infty} \frac{\partial \tau(q)}{\partial q}. \quad (11)$$

Therefore $\Delta\alpha \equiv \alpha_{\max} - \alpha_{\min}$ is another measure for quantifying multifractality nature of underlying data. The high value of $\Delta\alpha$ corresponds to more multifractal behavior.

B. Singular value decomposition

Recognizing trends and making proper detrending procedures are an important step toward robust analysis. Wu *et al.* [37] gave a statement accordingly; there is no unique definition of the trend. Subsequently, any proper algorithm for extracting trends from underlying data sets should remove embedded trends without destroying intrinsic fluctuations as much as possible. For real-world data sets the mentioned situation needs more precise considerations. It was demonstrated that MF-DFA is not able to eliminate the effect of intrinsic periodic trends in data series [38–40]. As a result, when MF-DFA applied to data with sinusoidal trends, spurious crossover occurs in the plot of fluctuation function. Hu *et al.* [39] showed that a periodic trend induces an artificial crossover at the scale of the sinusoidal periodicity. This crossover leads to difficulties in analyzing data in a sense that it makes the estimation of scaling exponent unreliable [41]. Therefore, to measure the scaling exponent correctly, we have to minimize the effect of such trends in the data before applying the MF-DFA. Along this line, various methods have been suggested including the Fourier filtering method [38,42], the empirical mode decomposition (EMD) method [43], and the singular value decomposition (SVD) technique [44]. Here we use SVD because, comparing with the other two techniques, it reduces both periodic and quasiperiodic trends in series with more than one peak in their power spectrums [44].

For a series $\{x_i\}_{i=1,\dots,N}$ with periodic or quasiperiodic trends, the steps of the filtering method based on SVD is as follows [44]:

(1) Find the number of periodic or quasiperiodic components of the data series using its power spectrum. This number is denoted by p .

(2) Construct the matrix $\Gamma = (\gamma_1, \gamma_2, \dots, \gamma_d)^T$, where $\gamma_k = (x_k, x_{k+1}, \dots, x_{k+N-(d-1)})$ and the superscript “ T ” represents the transpose operator. The dimension d of the matrix Γ is called the embedding dimension. Note that, for a power-law series, the embedding dimension should be chosen much larger than the number of frequency components p .

(3) Determine singular values in descending order by applying the SVD on the matrix Γ . Singular value decomposition of the matrix Γ is given by $\Gamma = U\Sigma V^T$, where U and V are two orthogonal matrices and Σ is the diagonal matrix whose eigenvalues are the desired singular values [45].

(4) Construct the filtered matrix $\Gamma^* = U\Sigma^*V^T$ with the new matrix Σ^* , which is obtained by setting the first $2p + 1$ eigenvalues of Σ to zero.

(5) Compute detrended data $\{x_i^*\}$, elements of the filtered matrix Γ^* , by mapping Γ^* back onto a one-dimensional series.

III. EXPERIMENTAL DATA

A home-built atomic force microscope operating in ultrahigh vacuum (UHV) at room temperature was used in experiments. Normal and lateral (i.e., friction) forces acting on the sensor tip are respectively proportional to normal bending and torsion of the cantilever beam and are measured

by means of an optical beam deflection scheme (with a four-segment photodiode). The experiments were performed on a NaCl single crystal, which was cleaved in air, transferred immediately to UHV, and annealed to about 100 °C for 30 min in order to remove contaminants. The preparation of samples under UHV conditions allowed the study of clean surfaces, free of water or adsorbates. Friction experiments were then conducted on dry and clean surfaces, without lubricants. We used silicon cantilevers consisting of single crystalline materials. The pyramidal tip is pointing toward the (001) direction and has a microscopic cone. At the apex, the cone angle is reduced and nominal tip radii of less than 10 nm can be obtained. For quantitative interpretation of friction force microscopy images, the normal and torsional bending of the cantilever have to be calibrated [46]. The normal spring constant k_N is given by

$$k_N = \frac{Ewt^3}{4l^3}, \quad (12)$$

where w is the width, l the length, t the thickness of the cantilever, and E the Young modulus of the material. For silicon, $E = 1.69 \times 10^{11}$ N/m². The thickness can be precisely determined from the resonance frequency f of the cantilever:

$$t = \frac{2\sqrt{12}\pi}{1.872^2} \sqrt{\frac{\rho}{E}} fl^2 = 7.23 \times 10^{-4} \frac{\rho}{m} fl^2, \quad (13)$$

where ρ is the mass density (silicon: $\rho = 2.3$ g/cm³). The relations between the deflection of the laser beam measured by the photodiode and the normal force acting on the tip can be obtained by recording deflection versus distance. The torsional spring constant k_T necessary for lateral force calibration is given by

$$k_T = \frac{Gwt^3}{3h^2l}, \quad (14)$$

where G ($=0.5 \times 10^{11}$ 3 N/m² for silicon) is the shear modulus.

In our case, the silicon cantilevers bearing the sharp tips are rectangular with a spring constant $k_N = 0.09$ N/m for normal bending and $k_T = 62$ N/m for torsion. These spring constants were calculated for the clamped beam geometry using optical microscopy data for the length and the width of the beam and the frequency of the first normal bending mode to determine its thickness.

The friction force is sampled on 256×256 grid points uniformly distributed on a 6×6 nm² area; see Fig. 1(a). In other words, the data set consists of 256 separate sets corresponding to 256 scan lines equally spaced by 6 nm/256 = 0.23 Å. Each scan line is 6 nm long and in the (001) crystallographic direction of the surface, meaning that at least 10 Na and 10 Cl ions are alternatively visited per scan. Along each scan line, friction is recorded at length steps of 0.23 Å. Figure 1(b) illustrates friction versus tip position along the scan line indicated by a dashed line in Fig. 1(a).

IV. RESULTS AND DISCUSSION

Now we investigate the scaling behavior and multifractal properties of atomic-scale friction by applying the MF-DFA1 method to our experimental data. As seen in Fig. 1(b), the

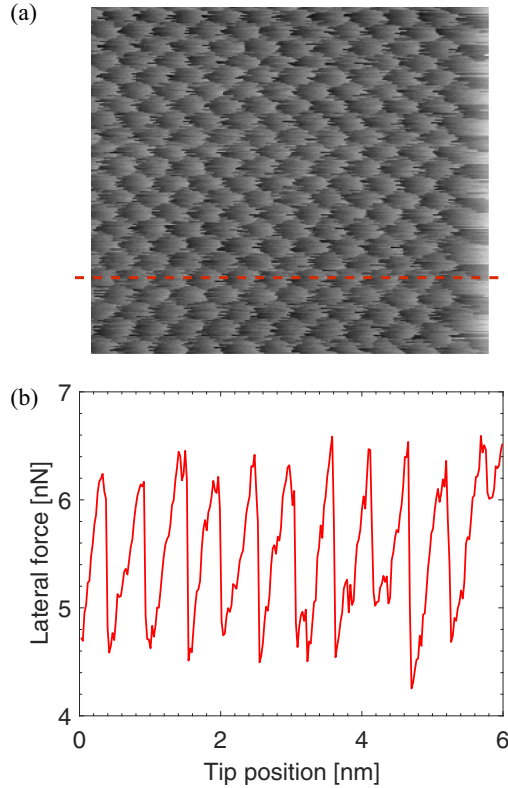


FIG. 1. (a) Lateral force map of NaCl surface at room temperature along (001) direction. (b) Friction versus the tip position along one of the scan lines shown by a dashed line in (a).

friction profile shows a quasiperiodic trend (or a sawtooth-like trend) whose periodicity is the same as the lattice constant of NaCl (0.56 nm) coming from the crystalline structure of the surface. Because of the periodic behavior, we expect to observe a crossover at the same order of the lattice constant in the plot of fluctuation function. Figure 2(a) depicts the log-log plot of $F_2(s)$ after averaging the fluctuation function over all 256 scan lines. In this figure, the length scale s varies from 10 to $256/3$. The upper curve of Fig. 2(a) is the result of applying MF-DFA to the original data. This curve clearly shows a crossover at the length scale $s_x \sim 0.6$ nm that happened, as expected, at a length scale comparable to the surface lattice constant $a = 0.56$ nm, i.e., the period of the atomic structure of the surface. The slopes of linear fits to the original data curve before and after the crossover are 1.10 ± 0.05 and 0.38 ± 0.01 at a 1σ confidence interval, respectively.

As stated earlier, applying MF-DFA to a data with periodic trends yields to unreliable scaling exponents. Thus, we need to remove such a sawtooth-like trend in our data, for which we use the SVD technique before applying the MF-DFA method. For SVD, the two parameters p and d should be adjusted. The value of p is determined from the number of peaks in the power spectrum, which is counted to be 2. Since, for SVD, a large embedding dimension ($d \gg p$) is desirable, we take $d = 100$. After removing the trend and applying MF-DFA, the fluctuation function for each scan lines is obtained. The lower curve of Fig. 2(a) represents the fluctuation function for the detrended data averaged over all scan lines. As seen,

by eliminating the trend, the *spurious* crossover vanishes and the fluctuation function shows a power law behavior. The scaling exponent $h(q = 2)$, which is the slope of the lower curve of Fig. 2(a), is obtained equal to 0.61 ± 0.02 at a 1σ confidence interval. Note that since the slope is less than unity, the Hurst exponent H becomes equal to $h(q = 2) = 0.61 \pm 0.02$. The value of $H = 0.61 \pm 0.02$ reflects the fact that the fluctuation of the nanofriction data is not a Gaussian white noise but a power-law correlated noise with positive correlation.

The computations carried out before this point, for determining the scaling exponent $h(q)$, are only for the certain value $q = 2$. However, in order to investigate the multifractal characteristics of the data, we should determine the scaling exponent $h(q)$ for other values of q . Figure 2(b) represents the generalized scaling exponent $h(q)$ as a function of moment q . In the case of the detrended data, $h(q)$ decreases monotonically with the moment. This strong dependence of $h(q)$ on q clearly represents the existence of multifractality in the nanofriction force data. According to Fig. 2(b), $h(q)$ has a stronger dependency on negative moments than positive ones. This, in turn, shows the greater role of small fluctuations in the multifractal properties of the series than large fluctuations.

The nonlinear behavior of the scaling exponent $\tau(q)$ also confirms the multifractality of the data; see Fig. 2(c). These characteristics of nanofriction force, nonlinearity and multifractality, can be more verified using the multifractal spectrum $f(\alpha)$, which measures the range of the fractal exponents in the series. Figure 2(d) shows $f(\alpha)$ as a non-convex function of singularity with a left truncation and the spectrum width $\alpha_{\max} - \alpha_{\min} = 0.58 \pm 0.08$. The spectrum width indicates the amount of deviation from monofractality. In other words, it provides a measure of multifractality: the more the width, the more multifractal are the series fluctuations.

The presence of scaling behavior in atomic-scale friction is the notable result of this study. The origins of scaling behavior at the atomic and mesoscale are fundamentally different. At the mesoscale, the scaling behavior is the result of the surface roughness. But, at the atomic scale where the surface is flat, the scaling behavior appears due to some fluctuation sources such as thermal and instrumental noises where their overall effect are usually assumed to be described by a white noise [6]. We found that this assumption is ruled out beyond a 5 interval over NaCl (001) surface at room temperature. Our work is only the proof of existence of noise correlation in the friction between two moving nanoscale objects. How this correlation is affected by, e.g., sample surface, tip velocity, and temperature are interesting questions worth separate studies following the procedure introduced in this work.

It should be noted that these results are not reliable for scales shorter than the so-called Markov length scale, which is the minimum length scale over which the data can be considered as a Markov process. This is due to the nature of profilometry measurement techniques in which there is an interaction between the probe's tip and the sample. For blunt tips, the convolution effect distorts measurements [47,48]. Fazeli *et al.* [49] showed that the tip size would affect only measurements in length scales smaller than the Markov length

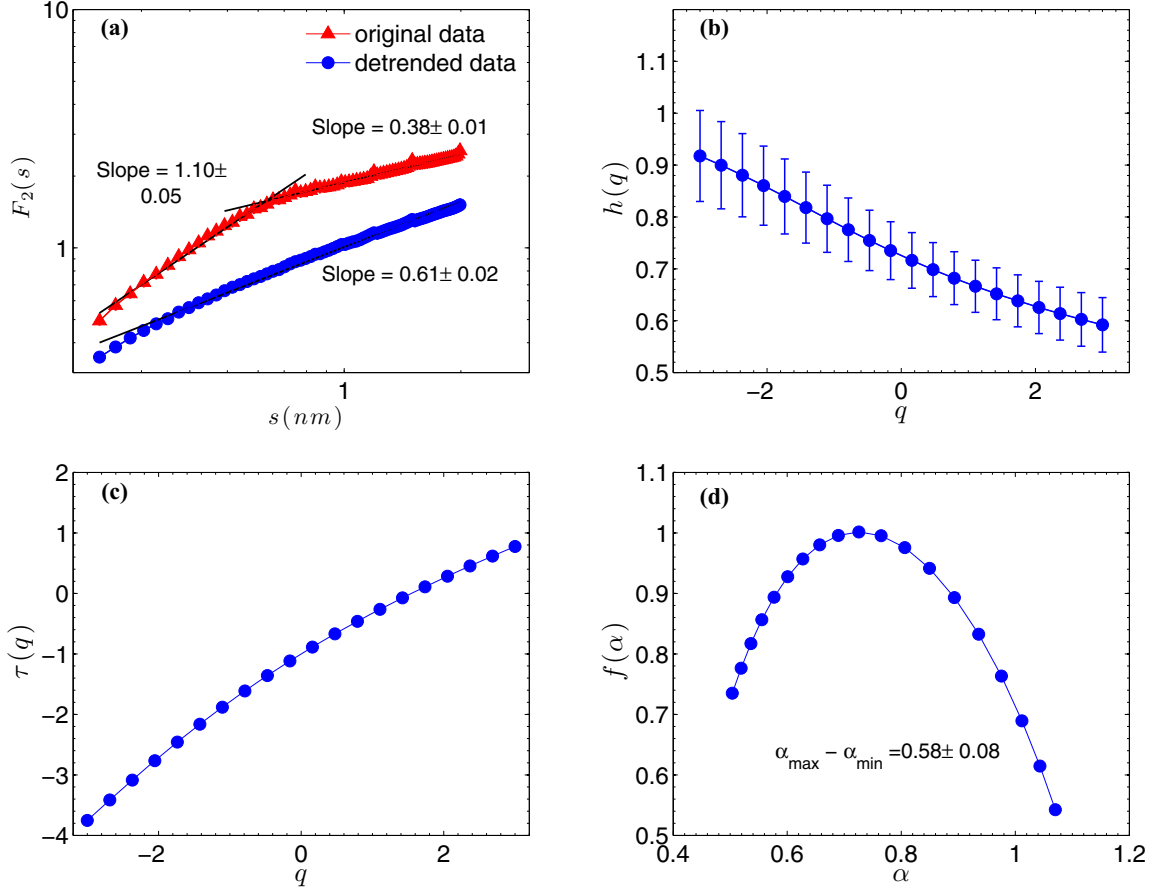


FIG. 2. (a) The log-log plot of MF-DFA1 function $F_2(s)$ versus scale s for original and detrended data of stick-slip friction force on NaCl. (b) Generalized scaling exponent $h(q)$ versus q for the detrended data. (c) The mass exponent $\tau(q)$ plot of nanofriction force. (d) The singular spectrum $f(\alpha)$ derived from the fluctuation of atomic friction force of NaCl for the detrended data.

scale. In other words, the scaling exponents obtained for length scales larger than the Markov length are unaffected by the mentioned phenomenon and therefore statistically reliable.

Here it is instructive to state briefly the procedure of determining the Markov length. In order to estimate the Markov length, shown here by l_M , for a given process $\{x(t)\}$, we exploit this fact that the necessary condition for $\{x(t)\}$ to be Markov is the Chapman-Kolmogorov equation [50–52]:

$$p(x_3, t_3 | x_1, t_1) = \sum_{x_2} p(x_3, t_3 | x_2, t_2) p(x_2, t_2 | x_1, t_1), \quad (15)$$

where $p(x_j, t_j | x_i, t_i)$ is the transition probability from the state x_i at initial time t_i to the state x_j at final time t_j . Note that this equation should be satisfied for any value of t_2 in the interval $t_1 < t_2 < t_3$; otherwise we say that $\{x(t)\}$ is a non-Markov process. We use the criterion

$$D(\tau) = \left| p(x_3, t_3 | x_1, t_1) - \sum_{x_2} p(x_3, t_3 | x_2, t_2) p(x_2, t_2 | x_1, t_1) \right| \quad (16)$$

to determine the Markov length scale. Here $\tau \equiv |t_3 - t_1|$. The Markov length l_M equates to τ for which $D(\tau) \rightarrow 0$.

Applying the above procedure to the nanofriction data, we find that the Markov length is $l_M \sim 0.08$ nm. The typical length scale in our study (0.2 to 2 nm) is quite larger than the obtained Markov length, demonstrating the reliability of our results.

V. SUMMARY

Friction between two contacting bodies emerges in a wide range of length scales from atomic to macroscales. At the mesoscopic scale, friction possesses a scaling behavior that originates in surface roughness. Consequently, at the atomic scale where there is no roughness anymore the question may arise: What is the scaling picture of friction at this scale? To address this question, we investigated the scaling behavior of the atomic-scale friction between the AFM tip and the flat surface of NaCl(001). The friction profile consists of fluctuations superimposed with a sawtooth pattern due to stick-slip motion. We used the singular value decomposition to filter out the trend, followed by the MF-DFA analysis on the clean data (fluctuations). As a result, the scaling behavior for the friction data ranging from 0.2 to 2 nm was observed, indicating that nanofriction fluctuations cannot be modeled by a white noise signal. In addition, the dependence of the generalized Hurst exponent $h(q)$ on the variable q means

that the scaling behavior of the data cannot be described by only one scaling exponent. Subsequently, our results showed the multifractal behavior of the combined noise contribution in nanofriction data (the original data reported by AFM).

This study could be extended to investigate the contribution of sample material, tip speed, scanning direction, and

temperature on the correlation and multifractality properties of nanofriction fluctuations.

ACKNOWLEDGMENT

The computational resources provided by the SARMAD cluster is acknowledged.

-
- [1] M. Urbakh and E. Meyer, *Nat. Mater.* **9**, 8 (2010).
- [2] C. H. Scholz, *Nature (London)* **391**, 37 (1998).
- [3] V. Bormuth, V. Varga, J. Howard, and E. Schäffer, *Science* **325**, 870 (2009).
- [4] B. Bhushan, *Introduction to Tribology*, 2nd ed. (John Wiley & Sons, New York, 2013).
- [5] A. Vanossi, N. Manini, M. Urbakh, S. Zapperi, and E. Tosatti, *Rev. Mod. Phys.* **85**, 529 (2013).
- [6] S. Yu. Krylov and J. W. M. Frenken, *Phys. Status Solidi B* **251**, 711 (2014).
- [7] D. G. M. Urbakh, J. Klafter, and J. Israelachvili, *Nature (London)* **430**, 525 (2004).
- [8] M. Evstigneev and P. Reimann, *Phys. Rev. B* **87**, 205441 (2013).
- [9] D. Mandelli, A. Vanossi, and E. Tosatti, *Phys. Rev. B* **87**, 195418 (2013).
- [10] M. Evstigneev, A. Schirmeisen, L. Jansen, H. Fuchs, and P. Reimann, *Phys. Rev. Lett.* **97**, 240601 (2006).
- [11] L. Prandtl, *J. Appl. Math. Mech.* **8**, 85 (1928).
- [12] G. T. Tomlinson, *London Edinburgh Dublin Philos. Mag. J. Sci.* **7**, 905 (1929).
- [13] Y. Sang, M. Dubé, and M. Grant, *Phys. Rev. Lett.* **87**, 174301 (2001).
- [14] L. Jansen, H. Hölscher, H. Fuchs, and A. Schirmeisen, *Phys. Rev. Lett.* **104**, 256101 (2010).
- [15] I. Barel, M. Urbakh, L. Jansen, and A. Schirmeisen, *Phys. Rev. Lett.* **104**, 066104 (2010).
- [16] E. Gnecco, R. Bennewitz, T. Gyalog, C. Loppacher, M. Bammerlin, E. Meyer, and H.-J. Güntherodt, *Phys. Rev. Lett.* **84**, 1172 (2000).
- [17] A. E. Filippov and V. L. Popov, *Phys. Rev. E* **75**, 027103 (2007).
- [18] V. L. Popov, J. Starcevic, and A. E. Filippov, *Phys. Rev. E* **75**, 066104 (2007).
- [19] O. Y. Fajardo, I. Barel, and M. Urbakh, *J. Phys.: Condens. Matter* **26**, 315005 (2014).
- [20] A. Labuda, M. Lysy, and P. Grütter, *Appl. Phys. Lett.* **101**, 113105 (2012).
- [21] A. Labuda, M. Lysy, W. Paul, Y. Miyahara, P. Grütter, R. Bennewitz, and M. Sutton, *Phys. Rev. E* **86**, 031104 (2012).
- [22] A. Labuda, J. R. Bates, and P. H. Grütter, *Nanotechnology* **23**, 025503 (2012).
- [23] Y. Dong, H. Gao, and A. Martini, *Europhys. Lett.* **98**, 16002 (2012).
- [24] Y. Dong, H. Gao, A. Martini, and P. Egberts, *Phys. Rev. E* **90**, 012125 (2014).
- [25] J. W. Kantelhardt, S. A. Zschiegner, E. Koscielny-Bunde, S. Havlin, A. Bunde, and H. Stanley, *Physica A* **316**, 87 (2002).
- [26] P. Norouzzadeh and G. Jafari, *Physica A* **356**, 609 (2005).
- [27] M. S. Movahed, G. R. Jafari, F. Ghasemi, S. Rahvar, and M. R. R. Tabar, *J. Stat. Mech.* (2006) P02003.
- [28] S. Shadkhoo and R. G. Jafari, *Eur. Phys. J. B* **72**, 679 (2009).
- [29] L. Hedayatifar, M. Vahabi, and G. R. Jafari, *Phys. Rev. E* **84**, 021138 (2011).
- [30] H. Dashtian, G. R. Jafari, M. Sahimi, and M. Masihi, *Physica A* **390**, 2096 (2011).
- [31] C.-K. Peng, S. V. Buldyrev, S. Havlin, M. Simons, H. E. Stanley, and A. L. Goldberger, *Phys. Rev. E* **49**, 1685 (1994).
- [32] M. S. Movahed and E. Hermanis, *Physica A* **387**, 915 (2008).
- [33] S. Hajian and M. S. Movahed, *Physica A* **389**, 4942 (2010).
- [34] G. R. Jafari, P. Pedram, and L. Hedayatifar, *J. Stat. Mech.* (2007) P04012.
- [35] P. Pedram and G. R. Jafari, *Int. J. Mod. Phys. C* **19**, 855 (2008).
- [36] J. Feder, *Fractals* (Springer, New York, 1988).
- [37] Z. Wu, N. E. Huang, S. R. Long, and C.-K. Peng, *Proc. Natl. Acad. Sci. USA* **104**, 14889 (2007).
- [38] R. Nagarajan and R. G. Kavasseri, *Int. J. Bifurc. Chaos* **15**, 1767 (2005).
- [39] K. Hu, P. C. Ivanov, Z. Chen, P. Carpena, and H. E. Stanley, *Phys. Rev. E* **64**, 011114 (2001).
- [40] Z. Chen, P. C. Ivanov, K. Hu, and H. E. Stanley, *Phys. Rev. E* **65**, 041107 (2002).
- [41] Q. Zhang, Y. Zhou, V. P. Singh, and Y. D. Chen, *J. Hydrol.* **400**, 121 (2011).
- [42] C. Chianca, A. Ticona, and T. Penna, *Physica A* **357**, 447 (2005).
- [43] N. E. Huang, Z. Shen, S. R. Long, M. C. Wu, H. H. Shih, Q. Zheng, N.-C. Yen, C. C. Tung, and H. H. Liu, *Proc. R. Soc. London A* **454**, 903 (1998).
- [44] R. Nagarajan and R. G. Kavasseri, *Chaos Solitons Fractals* **26**, 777 (2005).
- [45] G. H. Golub and C. F. V. Loan, *Matrix Computations*, 3rd ed. (Johns Hopkins University Press, Baltimore, 1996).
- [46] E. Meyer, R. Overney, K. Dransfeld, and T. Gyalog, *Nanoscience: Friction and Rheology on the Nanometer Scale* (World Scientific, Singapore, 1998).
- [47] J. Aué and J. T. M. D. Hosson, *Appl. Phys. Lett.* **71**, 1347 (1997).
- [48] P. Sangpour, G. R. Jafari, O. Akhavan, A. Z. Moshfegh, and M. R. R. Tabar, *Phys. Rev. B* **71**, 155423 (2005).
- [49] S. M. Fazeli, A. H. Shirazi, and G. R. Jafari, *New J. Phys.* **10**, 083020 (2008).
- [50] H. Risken, *The Fokker-Planck Equation* (Springer, Berlin, 1984).
- [51] R. Friedrich, J. Zeller, and J. Peinke, *Europhys. Lett.* **41**, 153 (1998).
- [52] R. Friedrich and J. Peinke, *Phys. Rev. Lett.* **78**, 863 (1997).